

DJEnsemble: On the Selection of a Disjoint Ensemble of Deep Learning Black-Box Spatio-temporal Models

Yania Molina Souto,
Rafael Pereira
LNCC-DEXL
Petropolis, Brazil
yaniams,rpereira@lncc.br

Rocío Zorrilla, Anderson
Chaves
LNCC-DEXL
Petropolis, Brazil
{romizc,achaves}@lncc.br

Brian Tsan, Florin Rusu
UC Merced
Merced, USA
{btsan,frusu}@ucmerced.edu

Eduardo Ogasawara
CEFET-RJ
Rio de Janeiro, Brazil
eogasawara@ieee.org

Artur Ziviani
LNCC-DEXL
Petropolis, Brazil
ziviani@lncc.br

Fabio Porto
LNCC-DEXL
Petropolis, Brazil
fporto@lncc.br

ABSTRACT

Consider a set of black-box models – each of them independently trained on a different dataset – answering the same predictive spatio-temporal query. Being built in isolation, each model traverses its own life-cycle until it is deployed to production. As such, these competitive models learn data patterns from different datasets and face independent hyper-parameter tuning. In order to answer the query, the set of black-box predictors has to be ensembled and allocated to the spatio-temporal query region. However, computing an optimal ensemble is a complex task that involves selecting the appropriate models and defining an efficient allocation function that maps the model frame to the query region.

In this paper, we present a cost-based approach for the automatic selection and allocation of a disjoint ensemble of black-box predictors to answer predictive spatio-temporal queries. Our approach is divided into two parts—offline and online. During the offline part, we preprocess the predictive domain data – transforming it into a regular grid – and the black-box models—computing their spatio-temporal learning function. In the online part, we compute a DJEnsemble plan which minimizes a multivariate cost function based on estimates for the prediction error and the execution cost – producing a model spatial allocation matrix – and run the optimal ensemble plan. We conduct a set of extensive experiments that evaluate the DJEnsemble approach and highlight its efficiency. We show that our cost model produces plans with performance close to the actual best plan. When compared against the traditional ensemble approach, DJEnsemble achieves up to 4X improvement in execution time and almost 9X improvement in prediction accuracy. To the best of our knowledge, this is the first work to solve the problem of optimizing the allocation of black-box models

to answer predictive spatio-temporal queries.

1. INTRODUCTION

As AI expands into wide economical and societal activities, an increasing number of AI models are developed and embedded in diverse applications, ranging from finance [40] to medical patient diagnosis [19]. A particular class of AI models aim to predict spatio-temporal phenomena, such as weather forecast and urban transportation [7]. A few examples include AccuWeather, Inc. [39, 1] and Zhang et al. [38] for temperature prediction; Google AI [2] and Souto et al. [21] for rainfall forecast; and models to alert against traffic accidents that combine environmental attributes, road conditions, and satellite images [35, 22]. In these scenarios, a learner captures data patterns that are both spatially and temporally correlated to the prediction. Moreover, the spatio-temporal learner improves its prediction accuracy by learning data patterns from observations captured at neighboring locations. These characteristics add special challenges to the traditional prediction problem.

From our personal experience, we have noticed that operational data is shared within large organizations according to the business needs and following proper access policies. This is not the case with models, whose sharing is less common. Data scientists tend to build and use their models for local applications, unintentionally “hiding” them from a wider use within the organization. To address this issue, we consider a paradigm where both data and models are shared in production. The assumption is that models have been trained and validated independently – as in a traditional machine learning life cycle [36] – and are integrated into applications as black-box functions. In this paradigm, challenges emerge in the model selection process to answer a given prediction query. Black-box models exhibit different performance due to variation in the predictor’s architecture, hyper-parameters configuration, and data samples observed during training [14]. Even when the hyper-parameters have been diligently tuned, newly arriving data may reflect new patterns—which can flag models for updating. Nevertheless, as it has been argued in Leszczynski et al. [17], one may keep the current predictor to avoid instability in production. Hence, when sharing models in production, one

must account with their varying performance in different regions of the domain.

To illustrate this paradigm, consider a weather forecast scenario in Brazil, in which three spatio-temporal predictors (STP) are available. The first STP by Souto et al. [21] is a ConvLSTM model for temperature and rainfall prediction trained on a slice of the CFSR dataset [27] covering a region of the Brazilian territory. The second STP is STCONVS2S [23], a deep learning model for spatio-temporal prediction with a different learning approach trained on the same dataset. Finally, the third STP [24] implements an artificial neural network trained with data produced by operational numerical weather prediction models covering the city of Rio de Janeiro. When a farmer planting vegetables in a mountainous region at an altitude of 800m in the Rio de Janeiro state looks for the weather forecast for her farm, how can she take advantage of the availability of these different predictors to obtain the most accurate prediction? While the first two STPs cover the farm location, the corresponding data is combined with data from many other locations that are far away. The third STP includes only data that is spatially closer to the farm. However, the difference in altitude may adversely impact its accuracy. The temporal aspect is also important because the data used for the third STP has higher frequency. Lastly, although the first two STPs are built on the same training data, their prediction time and memory usage are highly different.

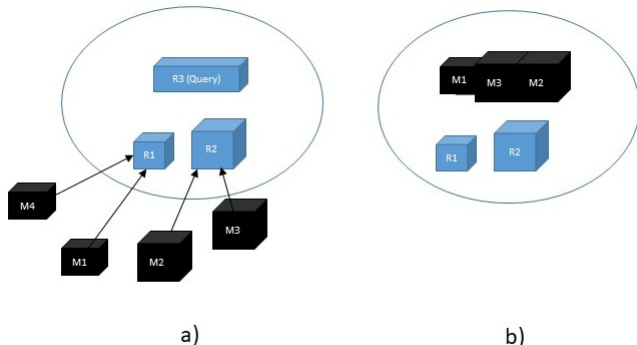


Figure 1: In Figure a), STPs M_1 and M_4 have been trained on Region R_1 , while STPs M_2 and M_3 have been trained on Region R_2 . A query Q is submitted on a different region, R_3 . Figure b) shows an STP composition allocating models M_1 , M_3 , and M_2 .

Abstractly, assume that a user has access to multiple black-box STP models that can answer predictive spatio-temporal queries. Then, the question is: “How to select the STP – or STP combination – that gives the optimal performance, where performance is measured as a function of multiple parameters, including accuracy, execution time, and resource utilization?” Our approach is to formulate and solve an optimization problem that finds the optimal STP ensemble of black-box predictors that minimizes a multivariate cost function. The solution specifies an allocation of the selected predictor’s spatial frames to the query region that form a disjoint allocation ensemble, as depicted in Figure 1. Identifying such an ensemble is, however, a hard problem as it involves: (i) estimating the prediction accuracy

of each black-box predictor at the query region; (ii) defining a black-box model ensembling strategy; (iii) finding the ensemble plan that minimizes the cost function; and (iv) planning for the execution of the ensemble.

In this paper, we present DJEnsemble, a novel method to solve the STP query optimization problem in order to build an ensemble that maximizes the performance of answering predictive spatio-temporal queries. Our method has two phases—offline and online. During the offline phase, we perform the following steps for each spatio-temporal domain:

- Cluster the domain time-series (see section 2) by the Generalized Lambda Distribution (GLD) probability density function parameters (see section 4.2.1) used to model the data distribution.
- Tile the spatio-temporal domain into a disjoint regular grid of time-series sharing the same cluster.
- Compute a centroid time-series as a representative for the set of time-series in each tile.
- Compute a learning curve for each black-box model that predicts its behavior as a function of the distance between the data distributions in the training and query regions.

Once the offline phase is complete, we can answer spatio-temporal predictive queries in the online phase as follows:

- Find tiles whose spatio-temporal region intersects within the query region.
- Select the models whose estimated error for the query region are below a threshold, using its learning curve function.
- Allocate each tile to the model that minimizes a multivariate cost function of the estimated error and execution cost.
- Build a disjoint STP ensemble plan based on the computed allocations.
- Execute the ensemble according to the plan and compose the overall prediction.

We perform extensive experiments that evaluate our approach on a real dataset and considering a set of STPs. Firstly, we show that the learning curve correctly approximates the prediction error as a function of data distribution distances. Next, we show that the optimization procedure implemented by the DJEnsemble approach is capable of selecting a good ensemble plan out of a large number of possible predictors allocations. The approach is resilient to different scenarios involving predictors’ architecture and training datasets. Finally, we compare the results obtained by DJEnsemble against the traditional ensemble approach. DJEnsemble achieves an accuracy improvement of up to 9X and it reduces query execution time by a factor of up to 4X.

2. PROBLEM FORMULATION

Consider a spatial Domain $\mathbb{D}(D, V)$, where $D = \{p_1, p_2, \dots, p_n\}$ is its discretization into a set of localized 2D-points $p_i(x_i, y_i)$, with x_i and y_i being spatial coordinates. At each point $p_i \in D$, observations are recorded as a time series V . Thus, an observation in V for spatial point p_i and time t_j is referred to as $v_{i,j}$. Additionally, we assume there are available black-box spatio-temporal predictors. The STPs are trained with datasets structured as a set of spatio-temporal series [6] $ST = (\langle x, y \rangle, V)$, where $\langle x, y \rangle$ corresponds to the spatial dimensions and V is a time-series of observations. For STPs, training and prediction, the data is preprocessed

as a list of bi-dimensional matrices (i.e frames), each holding data corresponding to a time instant and each of its cells holding a time-series at the corresponding spatio-temporal location. A STP receives a sequence of input frames $I = \langle I_1, I_2, \dots, I_n \rangle$ and produces a list of predictions as K output frames $O = \langle O_{n+1}, \dots, O_{n+k} \rangle$. Data in I contains the spatio-temporal observations from which predictions are to be made. For example, I may refer to the temperature in a spatial region during the last five days (i.e. number of I frames), and would predict the temperature in the same region for the next three days (i.e. three O frames).

As context, a user issues a spatio-temporal query $Q = \{R, ptime, V_q, Input, M_e\}$, where R is a 2D spatial region defined over the same domain \mathbb{D} , $R \subseteq D$. A region $R = (start, height, width)$ specifies a 2D location, $start$, and its orthogonal extension in a coordinate system. The size of R is given by its area, $height \times width$. Moreover, R can be split into subregions $R_{\#}$, $1 \leq \# \leq n$, such that $\bigcup_{\#=1}^n R_{\#} = R$ and $R_i \cap R_j = \emptyset, 1 \leq i, j \leq n, i \neq j$. $ptime$ defines the number of time-steps to be predicted, and V_q is a quantity to be predicted by the query, whose values are drawn from the time-series V . $Input$ is a dataset of time-series V in the spatial region delimited by R , and structured as frames I , which are input to a predictor. Finally, M_e is a performance metric, such as: *the mean square error; the prediction execution elapsed-time*, etc.

Consider again the farm scenario, which can be formalized as a query Q , where R specifies a mountainous area outside the city of Rio de Janeiro, $ptime$ is 3 days, V_q is the time-series of temperatures and $Input$ is a dataset of temperatures in R , and M_e is the root mean squared error function. To compute the predictions of V_q in query Q , we have three STPs $M = \{m_1, m_2, m_3\}$, where m_1 could be the ConvLSTM predictor presented in Molina et al. [21]. Each model $m_i \in M$ is associated with some metadata, including its training dataset (i.e a slice of the CFSR dataset). Thus, a model is specified as $m(Id, dataset, region, error-function, frame-size)$, where $region$ identifies a 3D *spatio-temporal* training region, $error-function$ specifies a learning curve, as the error estimate for a given data distribution distance (see section 4.2.3), and $frame-size$ is the product of the predictor’s frame width and height.

We formalize the *optimization of spatio-temporal predictive queries* (OSTEMPQ) problem as: given a spatial domain \mathbb{D} , and its discretization D ; a spatio-temporal query Q ; and a set of STPs M , determine an allocation $A = (R_{\#}, M')$, where $M' \subseteq M$ with $m_i \in M'$ and $\bigcup_{\#=1}^n R_{\#} = R$. Allocation A should be such that by invoking the models in M' produces a spatio-temporal prediction C that agrees with constraints in Q and exhibits an execution cost that minimizes M_e .

3. PRELIMINARIES

In this section, we present the types of spatio-temporal predictors considered in this work. Next, we briefly present the Generalized Lambda Distribution probability density function used to cluster data.

3.1 Deep Learning Model for spatio-temporal predictions

Deep learning spatio-temporal models have been extensively used in video and image analysis. Conv3D [31] was

the first successful convolution architecture to process large video datasets using only 3D convolution layers. The work has more than 1400 citations in Google scholar. It was followed by Tran et al. [32] where the authors suggest factorizing the space and temporal filters in two separate and consecutive components (2+1)D. We are interested in spatio-temporal regression models to solve problems such as weather forecast. One may apply the ARIMA (AutoRegressive Integrated Moving Average) model [5] to evaluate an autoregressive prediction for each time-series in the query region. More inline with our work, Shi et al. [29] developed a Convolution LSTM (ConvLSTM) based architecture. The architecture learns the spatial signals using a convolution operators followed by a recurrent neural network, applied to the prediction of rainfall. More recently, the Conv (2+1)D and CONVLSTM approaches inspired the STConvS2S model [23].

We consider using spatio-temporal deep learning models to solve regression problems, where the input is a list of fixed size frames and the output is also a list of frames of the same size as the input. The number of input frames determines the duration of the input temporal signal. Without loss of generality, we adopt the ConvLSTM architecture during our experiments. Given a particular ConvLSTM model with a fixed frame size and a spatial area where predictions should be computed, multiple invocations of the model may be necessary to cover the intended prediction area.

3.2 Modeling Data Distributions with GLDs

During training, a learner [28] captures the data patterns in an input dataset. Different approaches were proposed, to learn input data distributions [8] and extract metafeatures from the input training data [33]. We adopt the Generalized Lambda Distribution (GLD) probability density function (PDF) approach [25]. A GLD can model a family of data distributions, such as Gaussian, Logarithm, Exponential, etc. The function represents data distributions through the specification of lambda parameter representing statistical moments, where λ_1 and λ_2 determine location (distribution mean) and scale (standard deviation) parameters, while λ_3 and λ_4 determine the skewness and kurtosis of the distribution. A GLD is then represented as $GLD(\lambda_1, \lambda_2, \lambda_3, \lambda_4)$, known as the *RS* parametrization [25]. We fit GLDs to the distribution in the time-series at each spatial position [18]. Then, we use the λ parameters to identify regions sharing similar distributions, see section 4.2.1.

4. SOLVING THE OSTEMPQ PROBLEM

4.1 Solution Overview

Our approach to solve the OSTEMPQ problem observes the following constraints:

$$\begin{aligned} (i) & \forall R_i \in R_{\#}, \exists \text{ model } m_j \in M' \text{ such that } A(R_i, m_j); \\ (ii) & A(R_j, m_i) \wedge A(R_j, m_k) \text{ if only if } i = k. \end{aligned} \quad (1)$$

where A is a non-injective, non-surjective function. The solution has both an offline and online phase. During the offline phase, we preprocess data for a given domain, cluster regions of similar distribution, and restructure it into regular 3D tiles. Associated to each tile, a representative time-series is computed and models the data distribution at the tile spatio-temporal region. Additionally, for each model

in the set M , we build a learning function to estimate the model’s performance in different areas of the domain. Then, during the online phase, a cost function guides our search for ensembles that best answers a query.

Figure 2 depicts an overview of the system architecture implementing the DJEnsemble approach, including both the Offline and Online parts described in sections 4.2 and 4.3, respectively. The DJEnsemble approach has been implemented as an extension to the SAVIME system (see section 5).

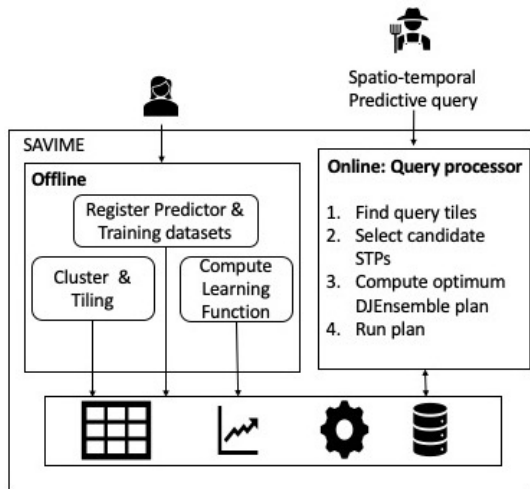


Figure 2: SAVIME system with support to the DJEnsemble query processing approach to solve the OSTEMPQ problem

Next, we detail the offline and online phases of the DJEnsemble approach.

4.2 Offline: Preprocessing

4.2.1 Clustering

We first perform clustering, to reduce the query evaluation space, by fitting a GLD function to each time-series V_i in domain D , associating the 4 GLD λ parameters to it. If V_i shows seasonality, we fit a GLD function to each season. Thus D is represented as $D_t(p, V, \lambda_1, \lambda_2, \lambda_3, \lambda_4)$.

After computing D_t , we cluster together time-series that have similar λ values, using *k-means*. We use the *silhouette* analysis to guide our choice of k . Thus, dataset D_t is transformed to $D_c(p, V, \lambda_1, \lambda_2, \lambda_3, \lambda_4, cid)$, where *cid* identifies the cluster each point belongs to.

Figure 3 shows the results of K-means clustering to the spatio-temporal dataset of temperature series in a region. Notice the non-convex regions with mixed data distribution defined by the clusters. The performance estimation of regular frame STPs for these regions are challenging.

4.2.2 Tiling

The spatio-temporal distribution of clusters is irregular and non-convex, so we restructure the data into regular tiles. Additionally, each tile would ideally contain data mostly from any single cluster. Inspired by the object detection method in YOLO [26], we start from some point $p_i((x_i, y_i), V_i)$, and aggregate neighbors to form a cube, as long as they are of the same cluster as p_i . We repeat until every point in D has formed a tile, thus producing *Tile(id,*

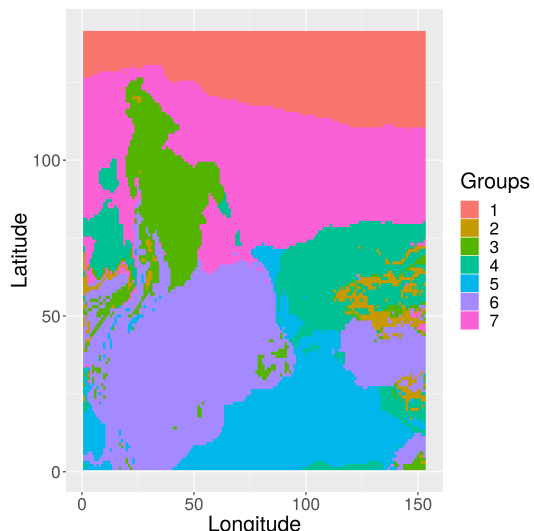


Figure 3: Clusters of a spatial domain, containing series of temperature values within a year. Silhouette analysis indicates 7 clusters.

$\langle coordinates \rangle, centroid$). *coordinates* are the 3D spatial region covered by a tile and *centroid* is the closest time-series to all other series in the tile. We use *centroid* as a representative of a tile’s data distribution.

4.2.3 Estimating model performance at query region

In addition to preprocessing the domain data, we estimate the performance of each candidate model at any region of the domain.

The experiments in section 6.2.1.1 show that one can compute a data distribution based prediction error function, see Equation 2:

$$E_{gnr} = F_e(dist_{i,j} + e_i) \quad (2)$$

For each candidate model, $F_e(dist_{i,j} + e_i)$ is a monotonic non-decreasing function. $dist_{i,j}$ is the distance between the distributions in the model’s training data d_i and a prediction region d_j . e_i denotes the model’s generalization error, obtained on the test set that the model was evaluated on. We assume that both the training and test sets have the same distribution. For a given model, we compute its $F_e(dist_{i,j} + e_i)$ learning function, by fitting a polynomial model to a series of pairs $(dist, error)$. It has been argued that learning curves that estimate a model loss as a function of increasing training data follows a power law [10]. We consider the increasing distance from a data distribution to be more analogous, and more precise, than the size of the training set, for predicting performance. Thus, find a polynomial function that maps data distribution distance to prediction error. The fitting process is as follows:

- Select regions with different data distributions than the one of the training data;
- Sequentially generate a modified version of these regions data by adding Gaussian noise, $r_i = r_{i-1} + \mathcal{N}(0, \sigma), 0 \leq i \leq n - 1$, with increasing σ values;
- Calculate the distance given using the DTW function applied over the centroid time-series (training data vs.

modified datasets), and compute the STP prediction error on the modified dataset;

- Train a polynomial regression model using the relation (distance, error), defining the fitting function: $error = F_e(dist_{i,j} + e_i)$;
- The polynomial regression model is defined by training the function in increasing order, until no improvement is observed;
- Using the fitted polynomial, as $F_e(dist_{i,j} + e_i)$, we can approximate the error when applying a model on unseen data.

Thus, at the end of the Offline part, we have organized the spatio-time series into tiles of homogeneous data distributions, represented by their centroid spatio-time series. Moreover, we have prepared an error generalization function predictor, for each registered spatio-temporal prediction model, parameterized by a data distribution distance between time-series. The latter is the fundamental piece in predicting the performance of a model in an unseen query region.

4.3 Online: Query Processing

The online phase of an approach to solve the OSTEMPQ problem is split into three phases: planing; execution; and post-processing. In the planing phase a set of black-box candidate predictors are selected and the allocation matrix is computed. Next, in the execution phase, models are evaluated according to the planned allocations. Finally, when necessary, post-processing actions are taken. The next section, discusses three approaches that can be used to solve the OSTEMPQ problem, following the above described execution phases.

4.3.1 Spatio-temporal model Ensemble

In the Online part of the OSTEMPQ problem, the spatio-temporal predictive query Q is solved. The domain has been partitioned into tiles T and there is a set of candidate models M to predict the query variable V . The *Traditional Ensemble* approach [37] solves query Q as follows. Firstly, in planning, it selects a subset $M' \subseteq M$ of models with testing performance greater than some threshold δ . It builds an allocation matrix, such that each model in M' completely covers the query region $Q.R$. Secondly, in execution, the allocations are submitted to an execution engine, such as Tensorflow. Finally, in post-processing, an aggregation operation computes a linear combination of the results. The *Traditional Ensemble* approach is depicted in Figure 4 a).

The *DJEnsemble* approach extends the planning phase. In addition to identifying the set M' that complies with the threshold δ , it computes the allocation matrix $A(R_{\#}, M')$ according to the constraints in Equation 1, and a cost function 3. The latter allocates the model with the minimum cost to each subregion $R_{\#}$. Next, the allocations in A are executed. Finally, the results obtained from the models are composed and returned as the query answer. An illustration of the approach is given in Figure 4 b).

For the *Traditional Ensemble* approach, in order to compute the predicted value $v_{i,j+1} \in V$, for time-step t_{j+1} at a point p_i on the query region $Q.R$, it runs all ensemble models and aggregate their predictions at each spatio-temporal position $\langle p_i, t_{j+1} \rangle$. In the *DJEnsemble* approach b), each predicted value $v_{i,j+1} \in V$ in $Q.R$ is the prediction of a single predictor allocated over the volume containing point p_i .

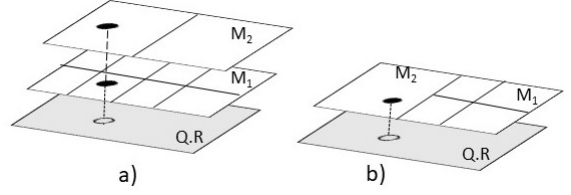


Figure 4: Spatio-temporal black-box models with different frame size. a) Spatio-temporal ensemble; b) Spatio-temporal DJEnsemble approach.

Finally, in a *Single Model* approach, the model with the best test results is allocated to cover all of query region $Q.R$. In this paper, we focus on the DJEnsemble approach, as depicted in Figure 4 b). We evaluate all three strategies and compare their results in 6.3.4.

4.3.2 Model Composition Search

Given the ensemble approach in 4.3.1, one must compute $S = (M, A)$, as proposed in section 2. Computing A requires considering the allocations of models in M over the query region $Q.R$. For each candidate model $m \in M$, with frame size m_{fs} ($m.frame-size$) a fraction of the query frame size $q_{fs} = (R.size)$, one may align its frame’s top-left corner to any of the p_i spatial positions in $Q.R$. This would continue until all points in $Q.R$ are considered for prediction by a model in M . This exhaustive procedure would hinder the ability to respond to online prediction queries. Instead, we consider structuring the domain into *tiles*, as described in 4.2.2. Given that each tile covers a region with time-series of similar data distribution, we can pick the model whose training data distribution resembles that of the tile’s centroid. This procedure reduces the search space to selecting candidate models for each query tile.

Given a suggested allocation, the implication of a possible difference between $m.frame-size$ and the tile size is managed as follows. Firstly, models are placed with top left corner matching that of the tile. Then for models whose frame size are a fraction of the tile size, we place as many non-overlapping instances of the model so that the tile region is covered. Conversely, in case the model frame extends beyond the tile area, we only consider predictions in spatial points falling within the tile area.

4.3.3 Cost Based Function

We designed a cost function to optimize model allocation. It is the linear combination of a model’s estimated generalization error and its estimated execution time. The error estimate is computed by the learning function, as described in 4.2.3. The estimate for the execution time is obtained by averaging the model’s previous recorded execution times, leading to an unitary cost (uc). Lastly, depending on the ratio between the model frame size and a tile’s 2D size, a number $\lceil r \geq 1 \rceil$ of invocations of the model is needed to cover all points in the tile region. In this case, each candidate allocation $A(t_i, m_j)$, for tile t_i , model m_j , and a weighting parameter μ_e , has a cost computed as depicted in Equation 3.

$$Cost_{i,j} = (1 - \mu_e) \times F_e(dist_{i,j} + \epsilon_i) + \mu_e \times \lceil r_{i,j} \rceil \times uc \quad (3)$$

4.3.4 DJEnsemble Algorithm

Algorithm 1 depicts the DJEnsemble algorithm. It receives as input: a query (Q); a set of tiles (T); a set of candidate models (M); an admissible error *threshold* and a normalization parameter (μ_e). The *DJEnsemble* function returns the set of mappings $A(T_i, M_j)$ that satisfies the constraints expressed in Equation 1 and minimizes a cost function, as detailed in Algorithm 2.

Algorithm 1 DJEnsemble algorithm

```

1: function DJENSEMBLE( $Q, T, M, threshold, \mu_e$ )
2:    $query_T \leftarrow queryTiles(Q, T)$ 
3:   for  $q_t \in query_T$  in Parallel do
4:     /* Obtain Query tile centroid */
5:      $q_c \leftarrow q_t.getcentroid()$ 
6:     /* Min priority queue */
7:      $pqi \leftarrow \perp$ 
8:     for  $m \in M$  do
9:       /* Obtain model centroid */
10:       $m_c \leftarrow m.getcentroid()$ 
11:      /* Compute distance between centroids */
12:       $dist \leftarrow DTW(m_c, q_c)$ 
13:      /* Compute prediction error estimate */
14:       $me \leftarrow m.error\_function(dist)$ 
15:      if  $me \leq threshold$  then
16:         $ex \leftarrow m.unitary\_cost$ 
17:         $mf \leftarrow m.framesize$ 
18:         $qtf \leftarrow q_t.framesize$ 
19:         $c \leftarrow cost\_function(me, mf, qtf, ex, \mu_e)$ 
20:         $pqi.push(c, < m, q_t >)$ 
21:      end if
22:    end for
23:    /*Collects best allocation */
24:     $S \leftarrow \bigcup_{i=1}^{|query_T|} pqi.top()$ 
25:  Return  $S$ 
26: end function

```

Algorithm 2 Cost Function

```

1: function COST_FUNCTION( $me, mf, qtf, ex, \mu_e$ )
2:    $r_{mf, qtf} \leftarrow \lceil \frac{qtf}{mf} \rceil$ 
3:    $cost \leftarrow (1 - \mu_e) \times (ex * r_{mf, t}) + \mu_e \times me$ 
4:   Return  $cost$ 
5: end function

```

The constraints in Equation 1 significantly reduces the search space. We adopt a greedy algorithm that selects for each tile the candidate model that minimizes the cost function, in Equation 3. In line 3, we fork a thread for each tile q_t . It then initializes a *Min priority queue* data structure. This is ordered by the estimated cost, keeping the minimum cost at each instant as the top element in the queue. In line 6, we iterate through the set of candidate models, $m_i \in M$. We obtain each model’s training data centroid and compute its distance to the query tile’s and the model’s centroid, lines 7 and 8. Next, we use the learning function, see section 4.2.3, to estimate the model m ’s generalization error on tile q_t . If the error is below some threshold, we evaluate the *cost function*, passing as parameters: the estimate for the model unitary execution time, the estimate for

the generalization error, the frames size, and a parameter weighting factor. The cost estimate is returned and placed in the priority queue, lines 10 to 15. In line 16, we compose an optimal plan with the minimum allocation for each tile.

5. SAVIME

We have integrated the DJEnsemble approach into SAVIME, an in-memory columnar multidimensional array data management system [20]. Given its multidimensional array data model, SAVIME suits storing spatio-temporal datasets, such as the meteorology dataset discussed in section 6.1.1. We also implemented the complete weather prediction scenario described in our motivating example in section 1.

To support black-box predictors, we developed a new prediction algebraic operator *predict*, which receives an array, and returns the results of the execution of the predictor, as an output array. The prediction functionality employs the *Tensorflow Extended* [4] platform to provide machine learning models as prediction services. Predictors are registered into the system through the REGISTER-MODEL operator. It receives parameters: the *model identifier*, the *input array type*, the *target attribute*, and the *input and output arrays dimension specifications*.

The CONV LSTM model discussed in the weather forecast motivating example is registered as follows:

```
REGISTER_MODEL(CONV LSTM, cfsrTar, "temperature",
               "tile-1|lat-35|long-40| time-10")
```

To invoke the registered ConvLSTM model for a given array region, we filter the desired region as a new array, according to our models input size, and inform the model identifier. For example, to obtain the temperature predictions for 10 days of a window whose coordinates are 6:40, 30:70, we use the Savime query:

```
PREDICT( SUBSET( cfsrTar, latitude, 6, 40,
                 longitude, 30, 70),
         CONV LSTM, "temperature" )
```

6. EXPERIMENTS

In this section, we evaluate the assumptions considered in this work and the applicability of the DJEnsemble approach. The following questions are evaluated:

- Is the *error_function* satisfactory to estimate the generalization error of a predictor in a query region?
- Do the offline steps improve the estimate of predictors error?
- Is the DJEnsemble approach resilient to variations in hyperparametrization and in training data?
- How does the DJEnsemble approach behave against baseline approaches?

Section 6.2 experimentally explores these questions.

6.1 Set-Up

6.1.1 Experimental Scenario

The data used in the experiments is a subset of the Climate Forecast System Reanalysis (CFSR) dataset with air temperature observations from January 1979 to December 2015, covering the space in 8N-54S and 80W-25W [27]. CFSR provides a homogeneous grid of daily temperature data. We

concatenate this information, obtaining 3D data with structure (day, latitude, longitude, temperature). This structure can be interpreted as a continuous series of temperature behavior in the last 30 years.

Seventeen models were created, using the ConvLSTM architecture (See Appendix Table 10). Models SA_1 to SA_6 share the same architecture (filters, layers, etc) and were trained in different regions. A second set, models DA_1 to DA_6 , were trained in different regions and with different architectures. Finally, model SR_1 is considered a baseline model and was trained in the region where the predictions are to be computed to answer the predictive query. In the training of models SA_1 to SA_6 and SR_1 , we use training regions whose time-series data distributions are very close and are modeled by a single distribution, whereas models DA_1 to DA_6 were trained in regions with multiple data distributions.

We specified Query Q over a synthetically built data region, designed to present controlled data distribution variation, within each query region tile. Thus, a tile t_i was selected from the spatio-temporal data domain obtained from the CSFR temperature dataset. The data distribution in t_i is represented by its centroid time-series. Then, we partitioned it into four disjoint sub-regions (see Figure 5): T_1 ($size = [10 \times 40]$), T_2 ($size = [10 \times 30]$), T_3 ($size = [8 \times 30]$), and T_4 ($size = [2 \times 30]$) and 200 time slots. The size of each tile is given in terms of latitudes and longitudes. Each point within a tile is separated from the others by 0.5 degrees and they were numbered to be indexed. A region of $[10 \times 10 \times 200]$ is a matrix (with 10 latitudes and 10 longitudes) with 200 temporal measure of temperature in each spatial point. We added Gaussian noise to each of sub-region, to simulate varying data distributions. The region comprising tiles t_i , $1 \leq i \leq 4$, is the target of the predictive query Q . In Figure 5, the gradation of the gray colors shows the intensity of the added noise. The intensity varies from 0.1 to 0.75.

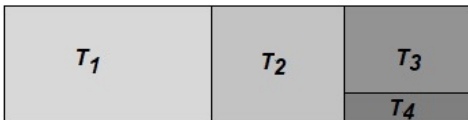


Figure 5: Predictive query. Each tile presents a slight variation in data distribution.

6.1.2 Computational environment

The computational environment was kept constant throughout the experiments: a Dell PowerEdge R730 server, with 2 CPUs Intel (R) Xeon (R) CPU E5-2690 v3 @ 2.60GHz; 768 GB of RAM memory; and running on a linux CENTOS kernel 3.10.0-1062. The Models were built and tested using a single NVIDIA Pascal P100 GPU, with 16GB RAM memory.

6.1.3 Methodology

Our evaluation of DJEnsemble considers the accuracy, root mean square error, and composition execution time, as discussed in equation 3. A model elapsed-time (ET) is computed by averaging its running elapsed-time for ten executions, at a single instant, for a unitary cost. The execution time (E_xT) is computed as $NE \times ET \times NTS$, where NE is the number of executions and NTS is the time interval to

forecast. The contribution of E_xT in Equation 3 becomes relevant when considering a set of candidate models with different architectures (i.e. variations on the CONVLSTM network hyper-parameters).

The model accuracy term composing the cost function in Equation 3 is measured as the root mean square error (RMSE) of the predictions. The estimate (S) for a model allocation RMSE is obtained by running the *erro_function* at each allocation. Complementary, the real RMSE (R) is obtained by running a model according to its allocation and comparing its predictions in a frame against the real values at each position of the query tile the frame has been allocated at and applying the RMSE equation. RMSE and execution time values are normalized by dividing by their maximum value respectively. Finally, the evaluation of DJEnsemble approach highlights three results: the estimated cost (S), given by the cost function and used to plan the execution; the real cost of the suggested plan (R), depicting the actual cost of running the model according to the allocation plan; and the Best Execution (BE) which gives the optimum real allocation for answering the query.

6.2 Results

6.2.1 Validation

An important assumption in this work is that in the context of auto-regression predictions, we can predict the error of a black-box model by a learning error function, mapping a data distribution distance to an estimate of the prediction error. The following experiments aim to validate this hypothesis.

6.2.1.1 Evaluating the learning curve extrapolation technique.

This experiment evaluates the correlation between data distribution distance and prediction error. Considering the data distribution to be univariate (e.g. temperature measurements), we use the paper running scenario based on the CSFR dataset. The computation of the error function follows the description in section 4.2.3.

Table 1 summarizes the experiment result. The distance values are taken relative to the data distribution in tile T_1 . The *DTW* column informs about the distance taken by applying the DTW function on the time-series of two tiles. Additionally, we adopt the *RMSE* to compute the prediction error on a tile, depicted in column *Error* of table 1. The Pearson correlation coefficient between the data distribution distances, columns *DTW* and the prediction error, column *Error*, is 0.88.

Error	Tile	Distance (DTW)
2.11	1	0
11.76	3	2.79665
18.22	2	2.95195
22.19	5	3.0207
26.68	6	3.01391
14.71	7	2.90363
23.53	4	3.03516

Table 1: Evaluation of the data distribution based error prediction driven approach, using Pearsons correlation and DTW distances relatives to tile T_1 .

Since there is a high Pearson correlation between the data distribution distance and the generalization error, we can fit a function $Error = F_c(dist_{i,j})$, as presented in section 4.2.3. Moreover, $Error = F_c(dist_{i,j})$ should be a monotonic non-decreasing function.

6.2.1.2 Distance to error model fitting.

In this experiment, we evaluate the *errorfunction* predictor. Figures 6 and 7 depict the generalization error curve for a set of black-box STP models $M = \{DA_1, DA_2, \dots, SA_1, \dots, SA_6\}$ obtained by applying the procedure described in section 4.2.3. In the y axis we plot the estimate for the generalization error, considering the RMSE in the spatio-temporal region being predicted (i.e. d_i , see section 4.2.3), and in the x axis, the corresponding distance of a region d_i to the base region d_0 , computed using the *DTW* function. One may observe that when the *DTW* distance passes the 10,000 mark, the accuracy clearly distinguishes models generalization capacity. In fact, the *error-function* estimates are used to prune models from the candidate space once the predicted generalization error crosses a *threshold*.

Table 1 shows that the data distribution distance is correlated to the prediction error. In Figure 6, we show that the error computed by the *error-function* can be used to order models for a given ST prediction. Moreover, the results in experimental section 6.3.2 shows that the error function reflects the generalization capacity of each model.

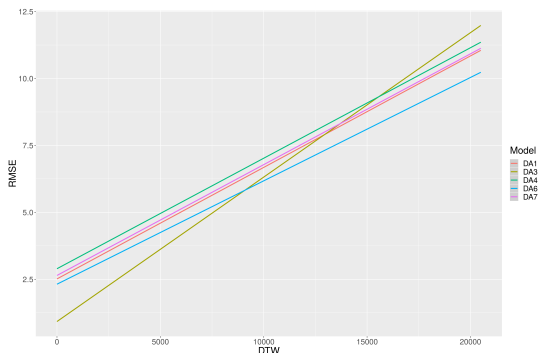


Figure 6: Curves representing generalization error growth produced by predictors with varying hyper-parametrization on increasingly noisy (distant) datasets .

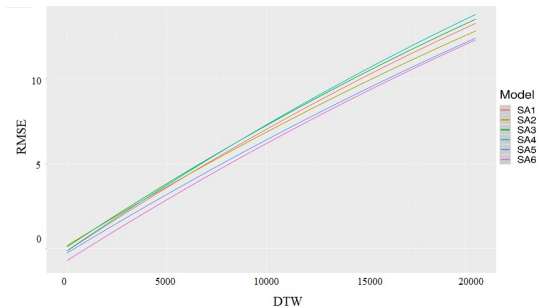


Figure 7: Curves representing generalization error growth produced by predictors sharing the same hyper-parametrization on increasingly noisy (distant) dataset.

6.2.2 The effect of tiling

As part of the DJensemble approach to solve the OSTEMPQ problem, we structure the data domain into regular tiles. The tiling process partitions the data domain into cubes of varying size. Each cube represents a spatio-temporal convex region sharing time-series with close data distribution among themselves. In this experiment, we evaluate the choice of model compositions when adopting the tiling approach against a domain discretization using a regular grid. Thus, we fix the requirement of having the domain structured into convex regions but relax the constraint of having cells sharing close data distribution. Thus, in the following experiment, we consider a small variation from the spatio-temporal predictive query described in Figure 5, as depicted in Figure 8. The cells indicated as $T_i, 1 \leq i \leq 4$, correspond to the tiling of the region, whereas the intervals denoted by $W_j, 1 \leq j \leq 4$, correspond to the tiling of the region as a regular grid.

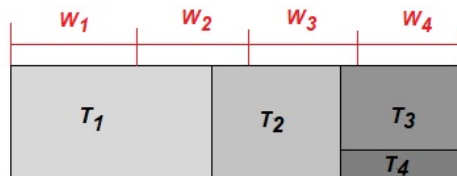


Figure 8: Prediction on a region partitioned on a regular Grid vs on a single distribution tiling.

Considering the relevance of data distributions in this discussion, we observe that the W_1 cell covers part of the area defined by T_1 , representing a single data distribution. W_2 and W_4 have a small fraction of their area with a second distribution, while W_3 covers regions with three different data distributions. Table 2 summarizes the results of applying six different models, each trained on regions disjoint from query region, for predictions on each of the cells in Figure 8. The values in Table 2 reflect the RMSE on temperature values.

M	W_1	T_1	W_2	T_2	W_3	T_3	W_4	T_4
DA_1	19.33	20.23	22.21	23.57	24.02	24.68	24.54	23.79
DA_2	81.07	81.09	80.84	80.73	80.72	80.7	80.71	80.74
DA_3	4.36	3.61	2.14	1.69	1.92	2.43	2.58	2.21
DA_4	6.38	5.17	3.79	2.79	2.46	2.11	2.56	2.91
DA_5	81.35	81.3	81.17	81.1	81.1	81.05	81.09	81.11
DA_6	19.08	20.1	21.98	23.49	23.88	24.53	24.51	23.75

Table 2: The effect of the tiling approach over model composition selection. Evaluating the results when the domain is structured into a cells of a regular grids against its structuring into tiles.

Initially, we analyze the effect of models evaluation on the W_4 cell against the $[T_3, T_4]$ tiles, as the regular grid cell W_4 covers the region splits into $[T_3, T_4]$. The best prediction for W_4 is given by model DA_4 with $RMSE = 2.56$. This is more 21.3% than $RMSE = 2.11$, produced by DA_4 in T_3 , and more 15.8% than $RMSE = 2.21$, produced by DA_3 in T_4 , and 18.5%, if we take the average of the RMSE between T_3 and T_4 .

When considering the best plan at each domain structuring, we have that for the regular grid, the best plan is:

$Best_W = [(W_1, DA_3), (W_2, DA_3), (W_3, DA_3), (W_4, DA_4)]$, while for the tiling structuring, the best plan is: $Best_T = [(T_1, DA_3), (T_2, DA_3), (T_3, DA_4), (T_4, DA_3)]$. Although the choices for the best plan are similar in both scenarios, the overall RMSE difference is of 14.1% for more accurate predictions in the tiling structuring. In all similar pairs of cells, but (W_3/T_3) , the one in tiling performed better than its counterpart in regular grid: $W_1/T_1 = 20.7%$, $W_2/T_2 = 26%$, $W_3/T_3 = 0.91%$ and $W_4/T_4 = 15%$. This is reassuring as the more precise structuring of the domain led to a better spatial positioning of the models, leading to an improved prediction performance.

6.3 Exploring different hyper-parameters and training dataset

These next set of experiments are divided into 4 stages, where we increasingly vary the differences among the black-box STPs, considering: the neural network hyper-parametrization; the training data distribution and the query region data distribution.

6.3.1 Single architecture, varying training data distributions and single tile for prediction

In this experiment, we consider 4 black-box STPs, $M = \{SA_1, SA_3, SA_4, SA_6\}$ sharing the same hyper-parametrization, but with different datasets used for training. The query T_1 tile is taken as the query region, thus both query region and training data are simply described by a single data distribution. Table 3 shows the results, where the column $Error(S)$ exhibits the prediction error computed by the *error-function*, while the column $Error(R)$, shows the actual error. Additionally, the *Distance* column shows the distance values computed by the *DTW* function. SA_3 and SA_4 show

Model	Distance	Error(R)	Error(S)
SA_1	2196.01	3.59	3.32
SA_3	1770.90	4.47	3.39
SA_4	1948.68	4.90	3.27
SA_6	42631.27	20.74	21.08

Table 3: Same hyper-parametrization and single query region data distribution. DTWs distances are calculated between the model training/validation region and query tile T_1 .

smaller *DTW*s distances because their training regions are closer to the query region in terms of data distribution. Due to this, when we use these models to predict in the query region we obtain the second and third best RMSE results, respectively. Another observation is given by SA_1 . The latter exhibits a distance greater than that of SA_3 and SA_4 , nevertheless with a smaller prediction error (real and estimate). The generalization of the SA_1 , SA_3 and SA_4 models can be seen in the Figure 6, where SA_1 presents a curve with less error than SA_3 and SA_4 for the measured distance values.

So far we conclude that, once divided into a cluster data region with similar distributions (*GLDs*) (see section 3.2), the *DTW* distance between the centroids of different regions is a good metric to compare 2 distributions. Besides that, the estimation function can be used to appraise the error in most cases. In the following sections we will use these two tools to create ensemble and model composition strategies.

6.3.2 Single architecture, varying training data distributions e multiple tiles for prediction

In this experiment, we consider a query with multiple tiles, for which we can assess the combination of models that minimizes a cost function, composed by the prediction error and model execution cost, see section 4.3.3.

For this experiment we fix the architecture for model set $M = \{SA_1, SA_2, \dots, SA_6\}$. The models were trained in different regions that do not match the query region. As the models are similar in terms of architecture and input data frame size, the execution elapsed-time and number of model instances invocations needed to answer the query are constant for all models per tile. For this reason, the execution elapsed-time is not considered in this experiment. We can reconsider our cost function as:

$$Cost_{mt} = \sum_{t=1}^n W_t (w_1 F_m(dist_{m,t} + \epsilon_m) + w_2 ET). \quad (4)$$

We add a sum operator as we want to optimize the prediction cost of all the tiles in the query and a constant W_t that represents the percentage of area that the tile covers over the query region ($[W_{T_1} = 0.4, W_{T_2} = 0.3, W_{T_3} = 0.24, W_{T_4} = 0.06]$). Again, the *DTW* distance is used to inform on the distances between the model training and query regions (See Table 4).

Model	T_1	T_2	T_3	T_4
SA_1	2008.88	2640.48	3215.50	2150.72
SA_2	49763.79	57445.83	61182.64	55608.07
SA_3	1813.04	2737.75	3200.94	2096.85
SA_4	1849.48	2519.36	3465.86	2220.04
SA_5	49554.81	57122.75	60786.23	56020.07
SA_6	47442.06	55341.19	57588.49	54560.79

Table 4: Data distribution distance between query tiles and training tiles. The latter were used to build models SA_1 to SA_6 .

We initially interpret the models distance with respect to the four query tiles. Table 4 highlights that the black-box STPs SA_1 , SA_3 and SA_4 were trained in regions whose data distribution are close to that of the query region, leading to smaller distances. The training region of model SA_3 shows the smallest distance among all models, except in T_2 where SA_4 has an even closer distribution. The complement to the distance information is given by the *error-function*. As before, in Figure 6, the generalization capacity of SA_1 is constantly higher than the other models. Thus, a decision based on Figure 6 would pick model SA_1 for all tiles, whereas the distance based information would weight towards SA_3 and SA_4 . Figure 9 depicts both the cost model estimate (S) and the real errors (R) for each model at each query tile. We observe that the cost model can easily discard models SA_2 , SA_5 and SA_6 . Additionally, the three remaining candidates are the ones with best execution results. Thus, the cost model narrowed down the set of candidate models to be used to answer the query.

Figure 10 summarizes the results from a full query region prediction point of view. The blue line shows the plan chosen by the cost model. The gray line shows the actual performance results obtained when running the cost function chosen plan. Finally, the orange curve depicts the actual best plan based on real errors. The separation between the

gray and orange lines gives an idea of the real loss of quality that we have when using the execution plan selected by our algorithm. As it can be observed, the predictions were very close to the actual error showing a nice calibration of the cost model and the error function.

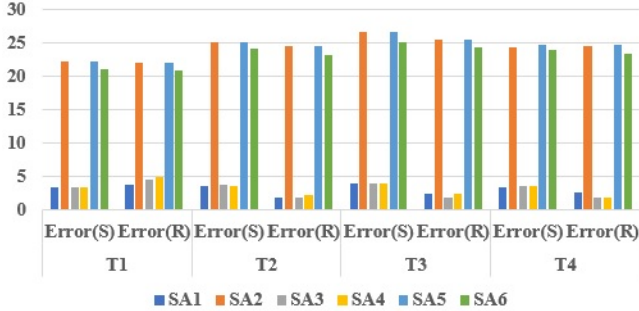


Figure 9: Prediction error, estimated by the cost-function(S) and evaluated by applying the model to the query region tile(R). Same hyper-parametrization and different training datasets.

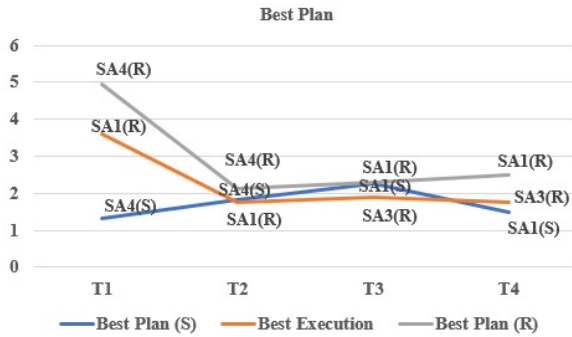


Figure 10: Comparison between the best plan chosen by DJEnsemble optimization vs the Best Execution (RMSE).

6.3.3 Multiple architectures, varying training datasets, each in a single tile, and multiple tiles for prediction

In this experiment, we add the execution cost to the cost function for selecting the model composition plan. We select 7 models with different architectures, DA_1 to DA_7 , and producing different execution times and performance. In this scenario the computational cost considers the use of memory and the number of invocations necessary for prediction. Both aspects are associated with the spatio-temporal regions covered by the model and the respective region of the query area to be predicted. In this context, our cost function expression considers the term involving the *ExecutionTime*.

$$Cost_{mt} = \sum_{t=1}^n W_t (w_1 * F_m(dist_{mt} + \epsilon_m) + w_2 * NE_{m,t} * ET_m) \quad (5)$$

Table 5 summarizes the DTWs distances, Table 6 shows models execution time and Figure 11 exhibits the errors of each model per tile, considering both actual model execution (R) and the estimates given by the cost function (S). The

weights w_1 and w_2 are defined in 0.7 and 0.3 respectively. Thus, we give greater importance to the prediction error in relation to the response time. In Table 5 we highlight in red the model with the closest data distribution per tile and in blue those for the second shortest distance.

Model	T_1	T_2	T_3	T_4
DA_1	47932.63	56040.44	58145.28	54743.67
DA_2	51401.98	58945.65	6290381	57095.19
DA_3	2432.30	4978.44	6821.75	4206.29
DA_4	2290.93	2438.26	2649.94	1916.10
DA_5	49641.91	57548.50	59953.10	56867.50
DA_6	47233.88	55391.31	57290.05	54146.01
DA_7	1813.04	2737.75	3200.94	2096.85

Table 5: Distances between the data distribution in the training dataset and the query region tile.

Table 6 summarizes the number of invocations required to complete the query tile regions $T = (T_1, T_2, T_3, T_4)$ based on the model input size and 200 predicted time slots. Additionally, the *ExecutionTime* (E_xT) is computed as $NE \times ET \times NST$, where NE is the number of invocations, ET is the elapsed-time of a single execution and NST is the number of time slot to forecast ($NST = 200$). We disregard the data transfer times and load time of the model as their data footprint are small. We have that the fastest two ($1^{st}/2^{nd}$) executions per tile are: $T_1(DA_3/DA_2)$, $T_2(DA_4/DA_3)$, $T_3(DA_4/DA_3)$, $T_4(DA_4/DA_3)$.

M	NE_{T_1}	NE_{T_2}	NE_{T_3}	NE_{T_4}	$ET \times NST(s)$
DA_1	2	2	2	2	3.63 ± 0.0365
DA_2	2	2	2	2	2.48 ± 0.0525
DA_3	2	2	2	2	1.49 ± 0.0430
DA_4	2	1	1	1	2.78 ± 0.0390
DA_5	4	3	3	3	2.16 ± 0.0455
DA_6	16	12	12	6	1.11 ± 0.0465
DA_7	4	3	3	3	1.25 ± 0.0465

Table 6: Evaluating the term execution time of the cost function Equation 2. NE is the number of invocations and ET is the model elapsed-time for 200 time slots.

Figure 11 summarizes the estimated and actual errors of each model by tiles. The first observation is that the error estimate is again very close to the actual computed errors. The models with closest data distributions were the ones that indeed exhibited the best actual performance, DA_7 and DA_4 . Additionally, Figure 6 shows that DA_3 exhibits a very good generalization capacity up to 9000 DTW distance, thus it also enters as a competitive model in our estimates.

Figure 12 shows the best plan, considering the cost function estimates (blue line), real execution of the cost based chosen plan (gray line) and overall best execution (orange line). In tiles T_1 , T_2 and T_3 , our cost model choice matches the best actual execution, (T_1, DA_3) , (T_2, DA_3) and (T_3, DA_7) . In T_4 , the errors of DA_3 and DA_7 are close to 1.76 and 2.21 respectively. We must remember that tiles T_3 and T_4 with dimensions (8x30) and (2x30), respectively, are smaller than the input size of the DA_3 (10x20) and DA_7 (10x10) models. In this case, it is necessary to extend the borders of the tile in the dimension of latitudes. This could cause distortion of the real error.



Figure 11: Models performance considering the RMSE, estimate (S) and real(R).

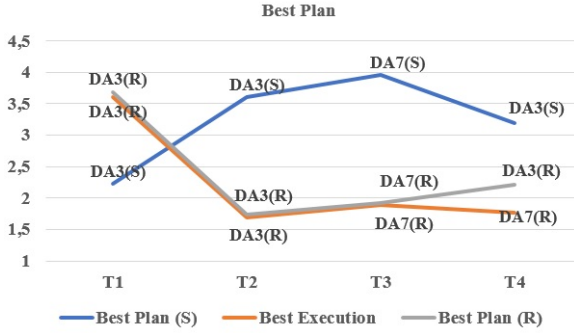


Figure 12: Comparison between the best plan chosen by DJEnsemble optimization vs the Best Execution (RMSE).

We compare our allocation $((DA_3, T_1), (DA_3, T_2), (DA_7, T_3), (DA_3, T_4)) = 2.35$ with the best allocation that can be generated from the set of available models, $((DA_3, T_1), (DA_3, T_2), (DA_7, T_3), (DA_7, T_4)) = 2.24$. In this experiment, the DJEnsemble approach obtains a plan 4.91% less accurate than the best model composition. Thus, in this experiment we observe that models with varying generalization error and hyperparameter can also be combined through the DJEnsemble approach. The best cost based plan achieves a performance 4.91% below that of the best execution. Moreover, the contribution of the execution time on the choice of the best plan is not significant as the fastest models are also DA_3 and DA_7 , which exhibit the best accuracy anyway, in this experiment.

6.3.4 DJEnsemble versus Baseline

We consider two main baseline approaches to solve the OSTEMPQ problem. The first approach would take a single model trained in the very same query region and use that model as a predictor for the query (i.e. single model approach). The second approach applies the Traditional Ensemble technique, as described in section 4.3.1.

6.3.4.1 Single model baseline.

The Single model baseline was constructed as follows. We used the SA_1 model architecture, which worked best in most experiments, and trained, validated and tested it in the same region specified in the query Q , using the time interval 1 to time-final - 200. The remaining time slots were used to for

the query.

The Table 7 summarizes the results of the best execution plan (DJEnsemble) against the baseline model created on the query data distribution.

DJEnsemble Plans	Error	Performance
1- ($'DA_3', 'DA_3', 'DA_7', 'DA_3'$)	2.35	18%
2- ($'DA_3', 'DA_3', 'DA_7', 'DA_7'$)	2.24	21.4%
Baseline Model	2.85	-

Table 7: Comparing the composition approach against a Baseline solution trained in the whole query region.

The first plan (1) was detected by our cost function. The underlined plan (2) corresponds to the best performing plan when we take into account all models. The values refer to execution errors produced by executing the plans. This result shows that the DJEnsemble approach can find compositions of black-box STP models exhibiting a performance improvement of 18% when compared against a single model baseline that has been built over the query region. The intuition for this result is that the disjoint ensemble of models offers a finer grain allocation of models to tile regions. Conversely, The single model baseline approach is less specific leading to less accurate predictions.

6.3.4.2 Ensemble baseline.

The second baseline technique considers the Ensemble approach. We built three ensembles and compare against the disjoint ensemble approach. We use six models from section 6.3.2 with similar architectures. The traditional ensemble is built using seven models, DA_1 to DA_7 . The second ensemble selected three models considering a cutting threshold of 5 degrees, computed using the error-function over DTW distances at each tile. The allocation, however, does not obey the tiling of the query region. Finally, our last approach selects models considering a cutting threshold of 5 degrees, computed using the error-function over DTW distances at each tile and used the tiling as the guide to model allocation. In addition, we built DJEnsemble plans. The (S) plan is a composition selected according to the approach based on estimated errors. Finally, a DJEnsemble (R) corresponds to a plan selected considering real errors. The results obtained by each strategy are shown in the Table 8.

Multiple models approaches	Error	Perf.	Exec.Time
1- Traditional Ensemble	21.03	-838.83%	68.35 \pm 0.586
2- Ensemble-DTW distance	3.07	-37.05%	34.38 \pm 0.482
3- Ensemble-DTW and Tiles	2.68	-19.64%	43.46 \pm 0.262
4- DJEnsemble (S)	2.35	-4.91%	14.06 \pm 0.193
5- DJEnsemble (R)	2.24	-	-

Table 8: Composition approach vs ensemble approaches.

We can observe that the more specific the allocation is the more accurate becomes the prediction. Thus capturing the data distribution in tiles and using it as the guide for selecting and allocating models pays-off. We can also observe a huge difference in latency. It is clear that the traditional ensemble approach requires running each selected model in the entire query region, each model being invoked as many times as needed to cover the query spatial region.

Additionally, the traditional ensemble approach requires a post-processing action to aggregate the values per prediction point and compute an average of the results. This leads to a performance penalty of almost 9x. It is interesting to observe that the usage of the DTW in filtering models in approach (2), significantly reduces the execution cost, as less models are run, but also makes the ensemble more specific, contributing to a more precise prediction. Incrementally going towards DJEnsemble, the approach (3) applies filtering and allocation per tile, showing competitive performance results. The latency results are slightly inferior than the one observed in (2). This can be due to a more frequent change in the execution context, as models are run per tile.

From the point of view of computational resources, each invocation of the prediction function takes up less than 256MB in memory. This would allow any of the execution plans of this work to be executed in parallel and the cost would be almost equivalent to the prediction time of the most-delayed model.

Best Plans	Error	Perf.	Exec.Time
DJEnsemble (DA_3, DA_3, DA_7, DA_3)	2.35	-	14.06 \pm 0.193
Single Model(SA_1 /Query region)	2.85	-21%	4.22 \pm 0.059
Ensemble-DTW and Tiles	2.68	-14%	43.46 \pm 0.262

Table 9: Best Plans

Finally, in Table 9, we select the best plan considering all approaches. As we can observe, DJEnsemble exhibits the best overall results in terms of prediction accuracy.

7. RELATED WORK

The adoption of the ensemble approach to improve the performance of weak learners is a common strategy to achieve more accurate predictions using black-box predictors. Approaches such as distillation [13] and fusion [11] and [30] are applied during model building and aim at producing a single new model. These approaches are orthogonal to DJEnsemble, as they could contribute with new models to the composition. Conversely, using a single model to predict in an area of varying data distribution produces less accurate predictions, as we showed in section 6.3.4.

Optimizations for training. Several works adopt techniques to efficiently perform feature extraction and feature selection with the purpose to generate models with high throughput and good accuracy [12]. The Rafiki system [34] uses distributed techniques for hyper-parameter tuning to select the best model parameters, store them along with the model architecture, task, dataset used and performance acquired. AutoGRD [8] is a meta-learning method for ranking the performance of learning algorithms. The datasets are characterized using a graph embedding representation (based on distribution and correlation between instances), in order to infer dataset similarity with regard to algorithm performance. In Willump [16] the authors use end-to end cascades approach to classify high permutation importance and low computational cost features to train models that achieves a desired accuracy target. Another work considering the cascade approach to optimize feature selection is Noscope [15], a framework application-driven that significantly reduce the cost of prediction serving for object detection in video streams.

Optimizations for Inference. In LASER [3], the authors exploit a form of model decomposition to incorporate feedback but not in real-time. LASER Serving is focused predictions from a single model.

Noscope [15] implements a set of techniques for significantly reducing the cost of prediction serving for object detection in video streams.

The framework Clipper [9] was designed to serve trained models at interactive latency. It implements two model selection policies based on multi-armed bandit algorithms, both span a trade-off between accuracy and computation overhead with adaptable batch sizes.

In Rafiki [34], the inference service provides real-time request serving by deploying the trained model. This system process the requests in the queue following FIFO, the objective is to maximize accuracy and minimize latency (exceeding time according to SLO). It supports two model selection approaches: single and multiple inference models based on ensemble techniques to ensure maximum accuracy.

Willump [16], improves ML inference performance by leveraging differing query modalities. Assuming ML models are used in higher-level end-to-end user queries in an ML application (compute the top-K predictions for a recommendation model) a query-aware adaptive parallelization.

DJEnsemble is specifically designed for spatio-temporal inference optimization. It uses a cost-based model to guide the selection and allocation of black-box predictors to a query region during the query plan phase. The approach could leverage inference optimization systems, such as Clipper and Rafiki. Some ideas from AutoGRD could be applied to extend DJEnsemble towards multi-variate predictions.

8. CONCLUSIONS

This paper presents the DJEnsemble, a disjoint model ensemble approach to plan for the composition of black-box deep learning models to answer spatio-temporal autoregressive predictive queries. The DJEnsemble approach includes an offline part, where data is structured into tiles, and an online part where a cost model is used to rank models to be allocated to each query tile, considering an estimate for the generalization error and models execution time. The results show that the approach largely exceeds traditional ensemble strategies both in accuracy (9x) and execution time (4x). There are plenty of future works to be explored. The disjoint model allocation to tiles may be flexibilized, particularly at tiles borders. The execution of the selected plans could take advantage of parallelism at the AI inference framework. Finally, another line of research involves exploring multivariate predictions and how to adapt the data distribution distance based approach for this scenario.

9. ACKNOWLEDGMENTS

Authors would like to thank CAPES and CNPq for scholarships and research productivity fellowships. They also thank Petrobras for financing this work through the Gypscie project. We also thank Artur Ziviani for comments at early stage of this work. Finally, Fabio Porto thanks the National University of Singapore and Prof. Beng Chin Ooi for hosting him during the paper preparation.

10. ADDITIONAL AUTHORS

11. REFERENCES

- [1] Using artificial intelligence to better predict severe weather: Researchers create ai algorithm to detect cloud formations that lead to storms., July 2019. www.sciencedaily.com/releases/2019/07/190702160115.htm, last access March 2020.
- [2] Using machine learning to nowcast precipitation in high resolution, January 2020. <https://ai.googleblog.com/2020/01/using-machine-learning-to-nowcast.html>, last access March 2020.
- [3] D. Agarwal, B. Long, J. Traupman, D. Xin, and L. Zhang. LASER: A scalable response prediction platform for online advertising. In *Proceedings of the 7th ACM International Conference on Web Search and Data Mining, WSDM 14*, page 173182, New York, NY, USA, 2014. Association for Computing Machinery.
- [4] D. Baylor, E. Breck, H.-T. Cheng, N. Fiedel, C. Y. Foo, Z. Haque, S. Haykal, M. Ispir, V. Jain, L. Koc, and et al. Tfx: A tensorflow-based production-scale machine learning platform. In *Proceedings of the 23rd ACM SIGKDD International Conference on Knowledge Discovery and Data Mining, KDD 17*, page 13871395, New York, NY, USA, 2017. Association for Computing Machinery.
- [5] G. E. Box, Jenkins, G.M, G. Reinsel, and G. Ljung. *Time Series Analysis: Forecasting and Control*. Wiley, USA, 2015.
- [6] R. Campisano, P. F. P. F. Borges, H., E. Paciti, Masegla, F., and E. Ogasawara. Discovering tight space-time sequences. In *Proceedings of the Int'l Conference in Big Data Analytics and Knowledge Discovery (DAWAK)*, Regensburg, Germany, 2018. Springer.
- [7] X. Cheng, R. Zhang, and W. Xu. Deeptransport: Learning spatial-temporal dependency for traffic condition forecasting. pages 1–8, 07 2018.
- [8] N. Cohen-Shapira, L. Rokach, B. Shapira, G. Katz, and R. Vainshtein. AutoGRD: Model recommendation through graphical dataset representation. In *Proceedings of the 28th ACM International Conference on Information and Knowledge Management, CIKM 19*, page 821830, New York, NY, USA, 2019. Association for Computing Machinery.
- [9] D. Crankshaw, X. Wang, G. Zhou, M. J. Franklin, J. E. Gonzalez, and I. Stoica. Clipper: A low-latency online prediction serving system. In *14th USENIX Symposium on Networked Systems Design and Implementation (NSDI 17)*, pages 613–627, Boston, MA, 2017. USENIX Association.
- [10] T. Domhan, J. T. Springenberg, and F. Hutter. Speeding up automatic hyperparameter optimization of deep neural networks by extrapolation of learning curves. In *Proceedings of the 24th International Conference on Artificial Intelligence, IJCAI15*, page 34603468. AAAI Press, 2015.
- [11] C. M. Gifford. *Collective Machine Learning: Team Learning and Classification in Multi-Agent Systems*. PhD thesis, University of Kansas, USA, 2009.
- [12] I. Guyon, S. Gunn, M. Nikravesh, and L. A. Zadeh. *Feature Extraction: Foundations and Applications (Studies in Fuzziness and Soft Computing)*. Springer-Verlag, Berlin, Heidelberg, 2006.
- [13] G. Hinton, O. Vinyals, and J. Dean. Distilling the knowledge in a neural network. In *NIPS Deep Learning and Representation Learning Workshop*, 2015.
- [14] D. Kang, R. Deepti, P. Bailis, and M. Zaharia. Model assertion for monitoring and improving ml models. In *Proceedings of the 2nd SysML Conference*, Paulo Alto, CA, 2019.
- [15] D. Kang, J. Emmons, F. Abuzaid, P. Bailis, and M. Zaharia. Noscope: Optimizing neural network queries over video at scale. *Proceedings of the VLDB Endowment*, 10(11):15861597, Aug. 2017.
- [16] P. Kraft, D. Kang, D. Narayanan, S. Palkar, P. Bailis, and M. Zaharia. Willump: A statistically-aware end-to-end optimizer for machine learning inference, 2019.
- [17] M. Leszczynski, A. May, S. Zhang, Wu, C. R. Aberger, and C. R. Understanding the downstream instability of world embedding. In *Proceedings of 3rd ML Sys Conf*, pages 1–13, Austin, Texas, USA, 2020.
- [18] J. Liu, N. M. Lemus, E. Pacitti, F. Porto, and P. Valduriez. Parallel computation of pdfs on big spatial data using spark. *Distributed and Parallel Databases*, 38(1):63–100, 2020.
- [19] X. Liu, L. Faes, A. Kale, S. Wagner, D. J. Fu, A. Bruynseels, and et al. A comparison of deep learning performance against health-care professionals in detecting diseases from medical imaging: a systematic review and meta-analysis. *The Lancet Health Digital*, 1(6):271–297, 10 2019.
- [20] H. Lustosa, F. Porto, and P. Valduriez. Savime: A database management system for simulation data analysis and visualization. In *Proceedings of the XXXIV Brazilian Symposium on Databases*, pages 85–96, Porto Alegre, RS, Brasil, 2019. SBC.
- [21] Y. Molina Souto, F. Porto, A. M. C. Moura, and E. Bezerra. A spatiotemporal ensemble approach to rainfall forecasting. In *Proceedings of International Joint Conference on Neural Networks (IJCNN)*, pages 1–8, Rio de Janeiro, 2018.
- [22] A. Najjar, S. Kaneko, and Y. Miyayaga. Combining satellite imagery and open data to map road safety. 2017.
- [23] R. C. Nascimento, Y. M. Souto, E. Ogasawara, F. Porto, and E. Bezerra. Stconvs2s: Spatiotemporal convolutional sequence to sequence network for weather forecasting, 2019.
- [24] I. Oliveira and C. Dos Santos. Post-processing of model data with machine-learning techniques for operational precipitation forecast. In *Proceedings of the 13th Conference on Artificial Intelligence*, January 2015.
- [25] J. S. Ramberg and B. W. Schmeiser. An approximate method for generating asymmetric random variables. *Commun. ACM*, 17(2):7882, Feb. 1974.
- [26] J. Redmon, S. Divvala, R. Girshick, and A. Farhadi. You only look once: Unified, real-time object detection. In *2016 IEEE Conference on Computer Vision and Pattern Recognition (CVPR)*, pages 779–788, 06 2016.

- [27] S. Saha and et al. Ncep climate forecast system reanalysis (cfsr) 6-hourly products, january 1979 to december 2010, 2010.
- [28] S. Shalev-Shwartz and S. Ben-David. *Understanding Machine Learning: From Theory to Algorithms*. Cambridge University Press, USA, 2014.
- [29] X. Shi, Z. Chen, H. Wang, D.-Y. Yeung, W. kin Wong, and W. chun Woo. Convolutional lstm network: A machine learning approach for precipitation nowcasting. In *Proceedings of the 28th International Conference on Neural Information Processing Systems*, pages 802–810, 2015.
- [30] S. P. Singh and M. Jaggi. Model fusion via optimal transport, 2019.
- [31] D. Tran, L. Bourdev, R. Fergus, L. Torresani, and M. Paluri. Learning spatiotemporal features with 3d convolutional networks. In *The IEEE International Conference on Computer Vision (ICCV)*, December 2015.
- [32] D. Tran, H. Wang, L. Torresani, J. Ray, Y. LeCun, and M. Paluri. A closer look at spatiotemporal convolutions for action recognition. In *2018 IEEE/CVF Conference on Computer Vision and Pattern Recognition*, pages 6450–6459, 2018.
- [33] R. Vainshtein, A. Greenstein-Messica, G. Katz, B. Shapira, and L. Rokach. A hybrid approach for automatic model recommendation. In *Proceedings of the CIKM 2018*, October 2018.
- [34] W. Wang, J. Gao, M. Zhang, S. Wang, G. Chen, T. K. Ng, B. C. Ooi, J. Shao, and M. Reyad. Rafiki: Machine learning as an analytics service system. *Proc. VLDB Endow.*, 12(2):128–140, Oct. 2018.
- [35] Z. Yuan, X. Zhou, and T. Yang. Hetero-convlstm: A deep learning approach to traffic accident prediction on heterogeneous spatio-temporal data. In *Proceedings of the 24th ACM SIGKDD International Conference on Knowledge Discovery & Data Mining, KDD 18*, page 984992, New York, NY, USA, 2018. Association for Computing Machinery.
- [36] M. Zaharia, A. Chen, A. Davidson, A. Ghodsi, S. A. Hong, A. Konwinski, S. Murching, T. Nykodym, P. Ogilvie, M. Parkhe, F. Xie, and C. Zumar. On challenges in machine learning model management. *IEEE Data Engineering Bulletin, Special Issue on Machine Learning Life-cycle Management*, 41(4), December 2018.
- [37] C. Zhang and Y. Ma. *Ensemble Machine Learning: Methods and Applications*. Springer Publishing Company, Incorporated, 2012.
- [38] Y. Zhang, S. Wistar, J. Li, M. A. Steinberg, and J. Z. Wang. Severe thunderstorm detection by visual learning using satellite images. *IEEE Transactions on Geoscience and Remote Sensing*, 55(2):1039–1052, 2017.
- [39] X. Zheng and et al. Detecting comma-shaped clouds for severe weather forecasting using shape and motion. *IEEE Transactions on Geoscience and Remote Sensing*, 57(6):3788–3801, 2019.
- [40] X.-l. Zheng, M. Zhu, Q.-b. Li, and Y.-c. Tan. Finbrain: when finance meets ai 2.0. *Frontiers of Information Technology & Electronic Engineering*, 20:914–924, 07 2019.

APPENDIX

Table 10 depicts the characteristics of the black-box deep learning models used throughout this paper.

Name	Filter Layer	Pattern	Input	Regions
SA_1, SA_2, SA_3	32	3	10	10x10 R_3, R_2, R_7
SA_4, SA_5, SA_6				R_4, R_5, R_{12}
DA_1	64	3	10	19x25 R_1
DA_2	32	3	15	19x22 R_2
DA_3	32	3	15	10x20 R_3, R_8
DA_4	64	3	10	10x30 R_4, R_{11}
DA_5	64	3	15	10x10 R_5
DA_6	45	3	15	6x5 R_6
DA_7	32	3	10	10x10 R_7
Baseline	32	3	15	10x100 QR
Region	Years	Latitudes	Longitudes	
R_1	31	21-41	16-41	
R_2	31	27-45	37-59	
R_3	18	131-141	30-50	
R_4	18	131-140	65-95	
R_5	5	0-9	143-154	
R_6	5	4-9	148-155	
R_7	18	125-135	80-90	
R_8	14	18-28	60-80	
R_9	12	15-25	0-10	
R_{10}	9	115-125	20-30	
R_{11}	7	55-65	0-30	
R_{12}	5	2-12	143-153	
QueryRegion(QR)	30	Disturbed region		

Table 10: Architectures and model training regions. The query region (Q.R) is extracted from latitudes: 131-141 and Longitudes: 30-130.